



# Glycosaminoglycans modulate long-range mechanical communication between cells in collagen networks

Xingyu Chen<sup>a,b</sup>, Dongning Chen<sup>a,c</sup>, Ehsan Ban<sup>d</sup>, Kimani C. Toussaint<sup>e</sup>, Paul A. Janmey<sup>a,f</sup>, Rebecca G. Wells<sup>a,c,g</sup> , and Vivek B. Shenoy<sup>a,b,1</sup>

Edited by David Weitz, Harvard University, Cambridge, MA; received September 10, 2021; accepted March 7, 2022

Cells can sense and respond to mechanical forces in fibrous extracellular matrices (ECMs) over distances much greater than their size. This phenomenon, termed long-range force transmission, is enabled by the realignment (buckling) of collagen fibers along directions where the forces are tensile (compressive). However, whether other key structural components of the ECM, in particular glycosaminoglycans (GAGs), can affect the efficiency of cellular force transmission remains unclear. Here we developed a theoretical model of force transmission in collagen networks with interpenetrating GAGs, capturing the competition between tension-driven collagen fiber alignment and the swelling pressure induced by GAGs. Using this model, we show that the swelling pressure provided by GAGs increases the stiffness of the collagen network by stretching the fibers in an isotropic manner. We found that the GAG-induced swelling pressure can help collagen fibers resist buckling as the cells exert contractile forces. This mechanism impedes the alignment of collagen fibers and decreases long-range cellular mechanical communication. We experimentally validated the theoretical predictions by comparing the intensity of collagen fiber alignment between cellular spheroids cultured on collagen gels versus collagen–GAG cogels. We found significantly lower intensities of aligned collagen in collagen–GAG cogels, consistent with the prediction that GAGs can prevent collagen fiber alignment. The role of GAGs in modulating force transmission uncovered in this work can be extended to understand pathological processes such as the formation of fibrotic scars and cancer metastasis, where cells communicate in the presence of abnormally high concentrations of GAGs.

matrix | force transmission | swelling | glycosaminoglycans

The extracellular matrix (ECM) in tissues and organs consists of collagen, enzymes, glycoproteins, and other macromolecules that provide structural and biochemical support to the cellular constituents. Structurally, the ECM is principally composed of an interlocking meshwork of collagen and glycosaminoglycans (1) (GAGs), which are large linear polysaccharides consisting of repeating disaccharide units. Collagen forms a cross-linked network of semiflexible fibers. A key feature of the fibrous nature of the collagen network is that cells can transmit and sense forces over distances much larger than their size (2). This long-range transmission of forces is necessary for various physiological and pathological processes. For example, cancer cells generate sufficiently high force to align nearby ECM fibers, which promote cell migration and the diffusion of growth factors from the tumor microenvironment (3). In general, collagen fibers reorient and align along the directions where the strains are tensile and buckle in the directions in which the strains are compressive. This mechanism allows the network to stiffen in an anisotropic manner along the direction of tensile principal strain as the network is deformed (2). The aligned fibers provide efficient paths for force transmission. The alignment of ECM fibers further increases cancer cell and ECM stiffness; therefore, the traction forces that the cells exert on the surrounding ECM create a positive feedback loop by up-regulating mechano-sensitive signaling, which further enhances the ability of the cells to exert forces (3). While previous studies have attempted to model the mechanical behavior and force transmission in tissues by considering the effect of GAGs (4, 5) interpenetrating the collagen network, the impact of GAGs on cellular force transmission remains unresolved.

Elevated levels of GAGs, specifically hyaluronic acid (HA), are observed in many types of tumors, wound sites, and other pathological processes such as fibrosis. In grade 3 human ovarian tumors, for example, median HA concentrations are 0.197 mg/mL (with a maximum of 4 mg/mL), more than 50 times higher than in benign tumors (0.003 mg/mL) (6). Excess HA accumulation has also been reported in human lung cancer, with a 4- to 200-fold increase (6), and in human prostate cancer, with a 7-fold increase (6). The distribution of HA varies significantly from point to point in the tumor microenvironment, and high concentrations of HA are associated with cancer

## Significance

Glycosaminoglycans (GAGs) are carbohydrates that are expressed ubiquitously in the human body and are among the key macromolecules that influence the development, homeostasis, and pathology of native tissues. Abnormal accumulation of GAGs has been observed in metabolic disorders, solid tumors, and fibrotic tissues. Here we theoretically and experimentally show that tissue swelling caused by the highly polar nature of GAGs significantly affects the mechanical interactions between resident cells by altering the organization and alignment of the collagenous extracellular matrix. The role of GAGs in modulating cellular force transmission revealed here can guide the design of biomaterial scaffolds in regenerative medicine and provides insights on the role of cell–cell communication in tumor progression and fibrosis.

Author contributions: X.C., D.C., E.B., R.G.W., and V.B.S. designed research; X.C., D.C., and E.B. performed research; P.A.J. contributed new reagents/analytic tools; X.C., D.C., E.B., K.C.T., P.A.J., R.G.W., and V.B.S. analyzed data; and X.C., D.C., E.B., K.C.T., P.A.J., R.G.W., and V.B.S. wrote the paper.

The authors declare no competing interest.

This article is a PNAS Direct Submission.

Copyright © 2022 the Author(s). Published by PNAS. This article is distributed under Creative Commons Attribution-NonCommercial-NoDerivatives License 4.0 (CC BY-NC-ND).

<sup>1</sup>To whom correspondence may be addressed. Email: vshenoy@seas.upenn.edu.

This article contains supporting information online at <http://www.pnas.org/lookup/suppl/doi:10.1073/pnas.2116718119/-DCSupplemental>.

Published April 8, 2022.

cell invasiveness. In breast tumors, the enrichment of HA has been observed exclusively at the leading edge of the tumor (7). The accumulation and localization of HA in stroma are linked to reduced survival (7), suggesting that HA participates in the generation of the precancerous stroma. A quantitative analysis of cellular force transmission in tissues with GAGs thus has the potential to provide insights into cellular mechano-sensing in pathological microenvironments.

HA is also enriched in cardiac tissues during development and after injury and is commonly used in tissue engineering constructs, often together with fibrous proteins. A recent study of cardiac myocytes in collagen-containing matrices showed that HA significantly decreased the force generated by the cell matrix constructs and inhibited the alignment of cardiac myocytes into integrated force-producing structures. HA has multiple cell receptors and can elicit intracellular signals, but in this study its effects were similar to those of the inert anionic polysaccharide alginate, suggesting that the effect of HA is predominantly physical rather than biochemical (8).

In this study, we developed a model that captures both the nonlinear strain stiffening behavior of the collagen network and the swelling induced by GAGs. We used this model to analytically and numerically predict the range of cellular force transmission in fibrous matrices that contain different concentrations of GAGs. Our model predicts that GAGs can significantly modulate long-range force transmission and mechanical communication between cells in collagen networks by making it difficult for fibers to align in an anisotropic manner. We quantitatively validated the theoretical predictions by examining the alignment of collagen fibers between cell spheroids cultured on collagen gels and collagen-HA cogels. Our work fills an important gap in understanding cellular mechano-sensing by shedding light on hitherto unexplored mechanisms of cellular communication in pathological conditions that involve GAG overproduction, including cancer, fibrosis, and wound healing.

## Results

**A Chemo-Mechanical Model of Cellular Force Transmission in Collagen Networks with Interpenetrating GAGs.** We considered the ECM as a mixture of three components: a solid component (collagen network with interpenetrating GAGs), an incompressible fluid component (interstitial fluid), and ions (cations and anions). GAGs contain many acidic groups (e.g., the carboxyl group on HA), which can dissociate into mobile protons and fixed negative charges (9). Each fixed negative charge requires a counterion nearby to maintain charge neutrality. In physiological conditions, the total ion concentration of the ECM is always greater than that of the external ionic solution (10). In vivo, external ionic strength is maintained by the circulatory system, including blood vessels and lymphatics. For example, sodium concentration is maintained at approximately 150 mmol/mL in blood (11). The difference between the ion concentration in the ECM and the surrounding environment gives rise to the well-known Donnan osmotic pressure (12), which drives water flux into the ECM. Since GAGs are large, charged molecules that are physically restrained in the dense collagen network, the influx of water can cause the ECM to swell. In the physiological state of 150 mmol/mL NaCl, the ECM is swollen, with a swelling pressure resisted by the elastic stress in the collagen-GAG solid matrix. Depending on the volume fraction of GAGs in the ECM and the concentration of ions in the surrounding environment, the matrix can swell to different levels as GAGs attract water into the matrix (Fig. 1A).

For example, Lai et al. (5) showed that collagen-HA cogels were swollen in hypo-osmotic solutions while collagen gels were not; the swelling also decreased with increasing ion concentrations in the external solution. Voutouri et al. (13) identified a linear correlation between tumor swelling and the ratio of HA to collagen content. To predict the impact of GAG-induced swelling on cellular force transmission, we developed a constitutive model for collagen-GAG cogels described by

$$\sigma_{ij} = g(F_{ij}, c_{col}, c_{GAG}, \bar{c}_{H^+}, \bar{c}_+, \bar{c}_-). \quad [1]$$

In this equation,  $\sigma_{ij}$  and  $F_{ij}$  denote the stress tensor and the deformation gradient of the collagen-GAG network, respectively. The parameters characterizing the cogels include concentrations of collagen ( $c_{col}$ ) and GAGs ( $c_{GAG}$ ) in the ECM and the concentrations of hydrogen ions ( $\bar{c}_{H^+}$ ), cations ( $\bar{c}_+$ ), and anions ( $\bar{c}_-$ ) in the surrounding environment.

To obtain the exact form of  $g()$  in Eq. 1, we considered three major mechanisms involved in the swelling process: 1) acidic groups on GAGs dissociate into fixed negative charges and mobile protons, increasing the ionic concentration in the matrix; 2) water flow into the matrix driven by Donnan osmotic pressure to compensate for the increased ion concentration; and 3) the network of collagen and GAGs is stretched as water flows in. To capture these mechanisms, we first incorporated the Donnan osmotic pressure induced by fixed negative charges and then introduced the constitutive relation of the collagen-GAG network that is stretched due to swelling. Using these constitutive relations, we simulated cell contraction in the cogels and studied the impact of GAGs on cellular force transmission.

**Swelling pressure induced by the GAGs.** GAGs contain acidic groups (e.g., carboxyl group) that can dissociate into mobile protons and negative charges ( $-COO^-$ ) fixed to the GAG chains (Fig. 1A). The dissociation can be calculated by the detailed balance condition that relates the concentrations of the reactants (undissociated acid groups) to the products (protons and carboxyl groups) (14),

$$\frac{c_{H^+} c_{COO^-}}{c_{GAG} D/J - c_{COO^-}} = N_A K_a. \quad [2]$$

Here  $c_{COO^-} = c_{H^+} + c_+ - c_-$  denotes the concentration of fixed charges (assuming electrical neutrality);  $c_{H^+}$ ,  $c_+$ , and  $c_-$  denote the concentration of protons, cations, and anions in the matrix, respectively;  $N_A$  denotes the Avogadro number; and the dissociation constant  $K_a$  is a measure of the strength of the acidic group;  $D$  denotes the number of acidic groups per unit mole of GAGs and  $J$  is the Jacobian denoting the ratio between the volumes of the gel after and before deformation. The fixed negative charges can cause an increase in the concentration of mobile positive ions in the matrix and attract water from the surrounding environment. The driving force for the inflow of water due to the imbalance of ion concentrations is the osmotic pressure,  $\Pi$ , that can be calculated using the relation (12) in the following equation:

$$\Pi = kT(c_{H^+} + c_+ + c_- - \bar{c}_{H^+} - \bar{c}_+ - \bar{c}_-). \quad [3]$$

Here  $\bar{c}_{H^+}$ ,  $\bar{c}_+$ , and  $\bar{c}_-$  denote the concentrations of protons, cations, and anions in the surrounding environment, respectively. The concentrations of ions within the matrix and in the external solution are related by the Donnan equations (12), which can be obtained by balancing the chemical potentials of the mobile ionic species in the ECM and in the external solution,

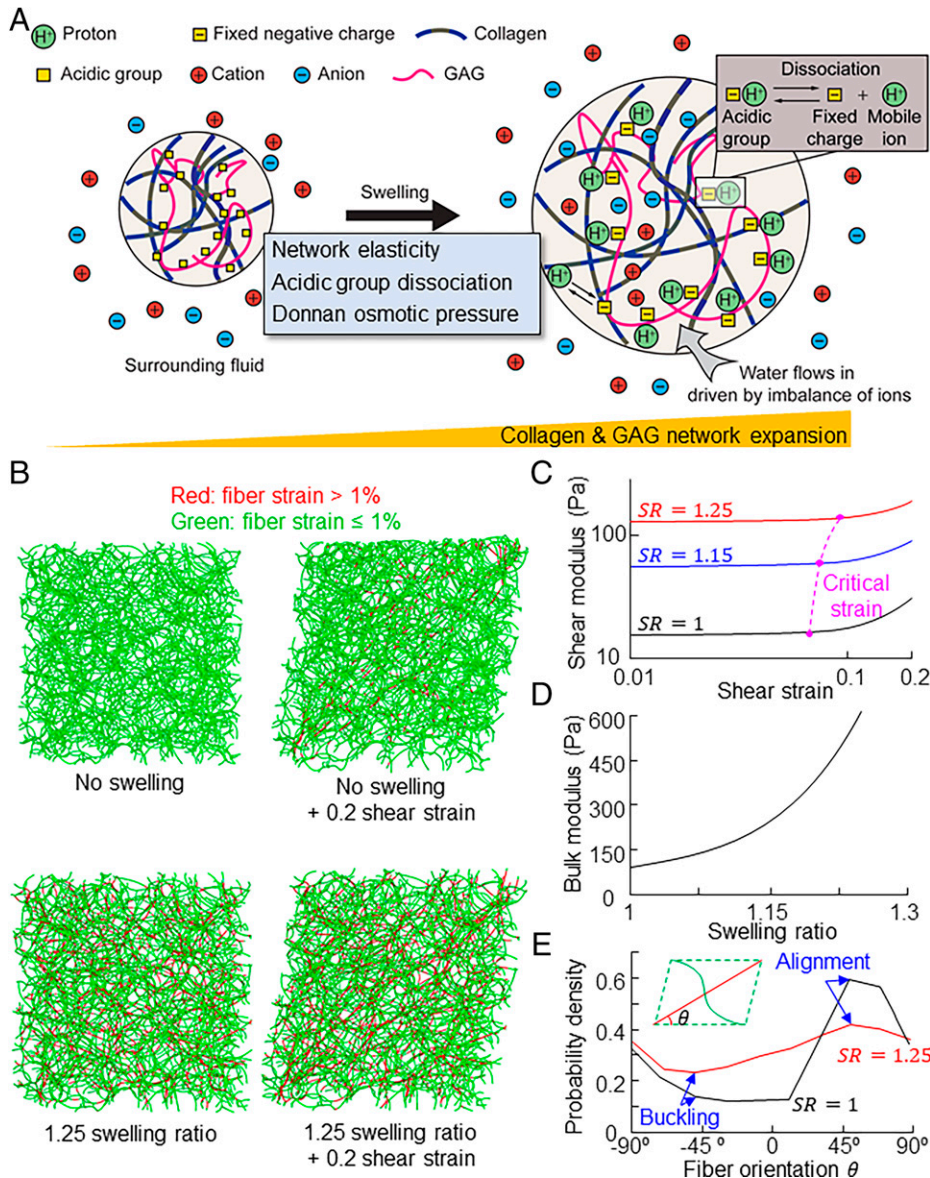


**Fig. 1.** (A) Schematic showing free swelling of a collagen-GAG gel. The carboxyl groups dissociate into negative charges that are fixed to the GAG backbone and protons in solution, which increases the osmolarity in the gel. Ions and water from the surrounding solvent flow into the gel (when the system reaches steady state). (B) Shows 3-dimensional discrete fiber simulations of random fiber networks before (Left) and after (Right) shear deformation (20% shear strain). The networks in the bottom row are swollen (25% volumetric strain) prior to the application of shear deformation. (C) Shear modulus as a function of the shear strain for networks with initial swelling ratios (SRs) of 1, 1.15, and 1.25, obtained from discrete fiber simulations. (D) The bulk modulus of the collagen network as a function of the SR. (E) Distribution of orientation of stretched fibers (strain > 1%) after 20% shear for networks with SR = 1 and SR = 1.25. The high (low) probability of stretched fibers along 45° (-45°) directions indicates fiber alignment (buckling).

$$c_+/\bar{c}_+ = c_{H^+}/\bar{c}_{H^+} \text{ and } c_-/\bar{c}_- = \bar{c}_{H^+}/c_{H^+}. \quad [4] \quad \text{in which}$$

Solving Eqs. 2–4 yields the expression of the swelling pressure induced by the acidic groups on GAGs (14),

$$\Pi = kT \left( c_{H^+} - \bar{c}_{H^+} + \left( \left( \frac{c_{H^+}}{\bar{c}_{H^+}} \right) - 1 \right) \bar{c}_+ + \left( \left( \frac{\bar{c}_{H^+}}{c_{H^+}} \right) - 1 \right) \bar{c}_- \right), \quad [5] \quad \text{and}$$

where

$$c_{H^+} = D \left( \sqrt[3]{-\frac{q}{2} + \sqrt{\left(\frac{q}{2}\right)^2 + \left(\frac{p}{3}\right)^3}} + \sqrt[3]{-\frac{q}{2} - \sqrt{\left(\frac{q}{2}\right)^2 + \left(\frac{p}{3}\right)^3}} \right) - \frac{N_A K_a}{3}, \quad [6]$$

$$p = -\frac{N_A K_a D c_{GAG}}{J} + \bar{c}_{H^+} \bar{c}_- - \frac{(N_A K_a)^3}{3D^3}, \quad [7]$$

and

$$q = -\frac{N_A K_a \bar{c}_{H^+} \bar{c}_-}{D^3 \left(1 + \frac{\bar{c}_+}{\bar{c}_{H^+}}\right)} + \frac{N_A K_a \left(\frac{N_A K_a D c_{GAG}}{J} + \bar{c}_{H^+} \bar{c}_-\right)}{3D^3 \left(1 + \frac{\bar{c}_+}{\bar{c}_{H^+}}\right)} + \frac{2(N_A K_a)^3}{27D^3}. \quad [8]$$

The above equation relates the osmotic pressure in the matrix to the ionic concentration of the external solution, the density

and strength of acidic groups on the GAGs, and the overall swelling ratio ( $J$ ), which in turn depends on the mechanics of the GAG–collagen network. This relation can be greatly simplified for in vitro and in vivo situations where the  $pK_a$  of the acidic groups is much smaller than the pH (see *SI Appendix, section 3*).

**The elasticity of the collagen network with interpenetrating GAGs.** Both the collagen network and GAGs contribute to the elasticity of the matrix. GAG chains interact with the collagen network through hydrogen bonds and electrostatic interactions (15, 16). In addition, GAGs can be covalently coupled to a core protein in vivo to form proteoglycans (17). Depending on the type of the core protein, proteoglycans can noncovalently bind to collagen fibrils (16). Given the interactions between the GAGs and collagen, it is reasonable to assume that GAGs and collagen undergo the same state of deformation on a macroscopic-length scale (on the order of cell dimensions ( $\sim 10$  to  $20 \mu\text{m}$ ) or more). We considered the strain energy density of the collagen–GAG network ( $W_E$ ) as the sum of the strain energy density of the collagen ( $W_{col}$ ) and the GAGs ( $W_{GAG}$ ):

$$W_E = W_{col} + W_{GAG}. \quad [9]$$

The mechanical behavior of the flexible GAG chains is dominated by their configurational entropy (18), which can be captured by the nonfibrous (Neo-Hookean) energy density function

$$W_{GAG} = \frac{c_{GAG}}{c_{GAG}^{ref}} \left[ \frac{\mu_{GAG}}{2} \left( \frac{\lambda_1^2 + \lambda_2^2 + \lambda_3^2}{J^{2/3}} - 3 \right) + \frac{\kappa_{GAG}}{2} (J - 1)^2 \right], \quad [10]$$

where  $\lambda_1$ ,  $\lambda_2$ , and  $\lambda_3$  denote the stretches in three principal directions and  $J = \lambda_1 \lambda_2 \lambda_3$  denotes the volume change as the matrix deforms. The stiffness of the GAG network depends on the concentration of GAGs; we explicitly scale the strain energy density with the concentration of the GAGs. Since GAGs in physiological conditions are dilute (on the scale of mg/mL), we explore the change of concentration in the physiologically relevant range by adopting a linear scaling relation to estimate the impact of concentration on stiffness. Here,  $c_{GAG}$  denotes the concentration of GAGs in the undeformed configuration and  $c_{GAG}^{ref}$  denotes a scaling factor that represents the GAG concentration at which the shear and bulk moduli are  $\mu_{GAG}$  and  $\kappa_{GAG}$ , respectively.

The collagen network was modeled using the constitutive relation we recently developed (2, 19, 20), which can account for the fact that collagen fibers can buckle, stretch, and align, depending on the nature of the applied stresses. When a randomly oriented collagen network is subject to a general state of stress, a portion of the fibers reorients and aligns along directions where the strains are tensile, while the rest of the fibers remain random (Fig. 1*B*). The alignment and concomitant stretching of fibers in tension make the network increasingly difficult to deform (Fig. 1*C*). In orientations where fiber strains are compressive, the fibers buckle and provide no resistance to deformation (Fig. 1*E*). Due to fiber realignment and buckling, the initially isotropic network stiffens in an anisotropic manner. We capture the strain-stiffening mechanism by writing the strain energy density function as a sum of the contributions from aligned fibers and unaligned fibers:

$$W_{col} = W_{aligned} + W_{unaligned}. \quad [11]$$

We used the nonfibrous material model (Neo-Hookean) to capture the isotropic mechanical behavior of the randomly aligned fibers and a highly nonlinear function  $f(\tilde{\lambda}_i)$  to capture the strain-stiffening effect induced by fiber alignment along tensile principal directions (*SI Appendix, Fig. S5*), as follows:

$$W_{unaligned} = \left[ \frac{\mu_{col}}{2} \left( \frac{\lambda_1^2 + \lambda_2^2 + \lambda_3^2}{J^{2/3}} - 3 \right) + \frac{\kappa_{col}}{2} (J - 1)^2 \right] s(J) \quad [12]$$

$$s(J) = \begin{cases} 1 & \text{for } J < 1 \\ J^\alpha & \text{for } J \geq 1 \end{cases} \quad [13]$$

$$W_{aligned} = \sum_{i=1}^3 f(\tilde{\lambda}_i), \quad [14]$$

$$f(\tilde{\lambda}_i) = \begin{cases} 0 & \text{for } \tilde{\lambda}_i < \lambda_L \\ E_f \frac{(\tilde{\lambda}_i - \lambda_L)^{n+2} (\lambda_U - \lambda_L)^{-n}}{(n+1)(n+2)} & \text{for } \lambda_L < \tilde{\lambda}_i < \lambda_U \\ E_f \left[ \frac{\lambda_U (\tilde{\lambda}_i - \frac{1}{2} \tilde{\lambda}_i^2)}{n+1} + \frac{(1 - \lambda_U + \tilde{\lambda}_i)^{m+2} - (m+2) \tilde{\lambda}_i}{(m+1)(m+2)} \right] & \text{for } \tilde{\lambda}_i > \lambda_U \end{cases} \quad [15]$$

Here,  $\tilde{\lambda}_i = 1 + \lambda_i - \frac{1}{3} \sum_{a=1}^3 \lambda_a$  denotes the deviatoric part of the principal stretch.  $\mu_{col}$  and  $\kappa_{col}$  are the shear modulus and bulk modulus of the unaligned “background” fibers, respectively;  $E_f$  characterizes the stiffness attributed to the network due to fiber realignment;  $m$  is the strain-stiffening exponent;  $\lambda_C$  denotes the critical stretch that characterizes the transition to alignment; and  $\lambda_L = \lambda_C - (\lambda_C - 1)/8$  and  $\lambda_U = \lambda_C + (\lambda_C - 1)/8$  denote the lower and upper bounds of the transition range  $\lambda_L < \tilde{\lambda}_i < \lambda_U$ , respectively. Once the tensile principal strain goes beyond the transition range, the fibers start to reorient and align with the tensile principal directions, and  $n$  is an exponent that characterizes the increase in strain energy in the transition range.

When the network experiences volumetric change induced by swelling, the fibers experience tensile forces irrespective of their initial orientation. We found through discrete fiber simulations that the network becomes stiffer in an isotropic manner without fiber alignment. In this case, both the shear modulus (Fig. 1*C*) and the bulk modulus (Fig. 1*D*) increased with swelling. To capture this effect, we added an additional scaling factor  $s(J)$  that only depends on the volumetric change given by Eq. 13. The parameter  $\alpha$  characterizes the nonlinear relation between collagen network isotropic stiffness and swelling. Note that in swollen states, the level of shear or uniaxial loading needed to align fibers is no longer  $\lambda_C$  (using the swollen state as the reference configuration, Fig. 1*C*). The fibers in the network are more difficult to align because fibers are stretched by the GAG-induced swelling and are more resistant to buckling; thus, a higher level of loading is needed to overcome the tension in the network. To illustrate this point, we compared the orientations of fibers in swollen and unswollen networks using discrete fiber simulations (Fig. 1*E*). Under the same level of shear strain, a lower percentage of the fibers aligned along the  $45^\circ$  orientation (direction of maximum principal stretch) for the swollen network. The distribution of fiber orientation is flat, indicating that the anisotropy of stiffness decreases with volumetric expansion. As a result, the critical strain needed for fiber alignment increases with the network volumetric expansion (Fig. 1*C*). Since in this study we focused on moderate levels of swelling ( $\sim 15\%$  swelling) where the critical strain varied slightly, we kept  $\lambda_C$  constant and used the criterion  $\tilde{\lambda}_i > \lambda_C$  to determine whether the fibers became aligned at a given material point. Note that the parameters  $\mu_{col}$ ,  $\kappa_{col}$ ,  $E_f$ , and  $\lambda_C$  in Eqs. 12–15 depend on the concentration of collagen,  $c_{col}$ . For example, previous studies have identified that the pore size of a collagen network, which determines the critical strain  $e_c$ , is inversely

proportional to the square root of the collagen concentration (21, 22). In this study, we conducted experiments to calibrate the model specifically for a fixed collagen concentration,  $c_{col} = 2.5 \text{ mg/mL}$ .

With the strain energy density of collagen and GAGs, the stress that arises from the elasticity of the matrix  $\sigma_{ij}^E$  can be calculated as

$$\sigma_{ij}^E = \frac{1}{J} \sum_{a=1}^3 \frac{\partial W_E}{\partial \lambda_a} \lambda_a n_i^a n_j^a, \quad [16]$$

where  $\lambda_a$  ( $a = 1, 2, 3$ ) and  $n_i^a$  denote the stretches and the unit vectors along the three principal directions, respectively. Combining the swelling pressure (Eq. 5) with the elasticity of the matrix (Eq. [15]), we obtained the overall stress ( $\sigma_{ij}$ ) in the ECM, which can be written as

$$\sigma_{ij} = \sigma_{ij}^E - \Pi \delta_{ij} - \Pi_{col} \delta_{ij}. \quad [17]$$

Here, we add an additional term  $\Pi_{col}$ , which can capture the swelling pressure induced by collagen. Collagen fibers are also charged (23), which may cause swelling with the same mechanism as GAGs.

Having developed the model, we first used this constitutive model to predict the dependence of the free swelling behavior on the GAG concentration. Next, by comparing the swelling ratio and the shear stiffness of the collagen–GAG network with experiments, we determined the parameters in our constitutive model.

**Collagen Matrix Swells Due to Osmotic Pressure Induced by GAGs.** We started analyzing the impact of GAGs by considering the case of free swelling where the ECM was subject to no constraining forces. Since ion concentrations are maintained at a relatively constant level in physiological conditions, we set  $\bar{c}_{H^+}$ ,  $\bar{c}_+$ ,  $\bar{c}_-$  on the outer boundary to be 0.0001 mmol/L (pH = 7), 150 mmol/L, and 150 mmol/L, respectively. Enforcing the conditions of mechanical equilibrium,

$$\frac{\partial \sigma_{ij}}{\partial x_j} = 0, \quad [18]$$

led to  $\sigma_{ij} = 0$  throughout the gel (14) and  $\sigma_{ij}^E = \Pi \delta_{ij}$  (Eq. 17), where  $x_j$  ( $j = 1, 2, 3$ ) denotes the spatial coordinates. This result suggests that the swelling pressure  $\Pi$  induced by GAGs leads to isotropic tensile stress on the solid matrix, leading to elastic deformation of the collagen–GAG network. Since the swelling pressure  $\Pi$  (Eq. 5) depends on the GAG-induced imbalance of ion concentrations across the network boundary, our model predicted that high concentration of GAGs,  $c_{GAG}$ , can induce high swelling pressure  $\Pi$  and thus requires a large solid matrix stress  $\sigma_{ij}^E$  to balance it, causing the expansion of the whole network.

To verify the prediction that GAGs can induce swelling of the collagen network, we conducted free swelling experiments using collagen–HA gels (see *Materials and Methods*). Notably, we used non-cross-linked HA of large molecular size (1.5 MDa). We expected that the HA chains were physically trapped inside the collagen mesh. HA contains carboxyl groups (24) that can dissociate into fixed negative charges and mobile protons, increasing the ion concentration within the collagen–HA gel. The imbalance of ion concentrations inside and outside the gel can drive in water and expand the collagen–HA gel (Fig. 2A). We found that while the collagen gels only showed negligible swelling ratios (defined in *Materials and Methods*, Eq. 21) of  $1.04 \pm 0.03$ , the collagen–HA gels were significantly more swollen (Fig. 2A). The source of swelling of the pure-collagen gel could be charges on collagen fibers, attracting water with the same mechanism as GAGs, captured

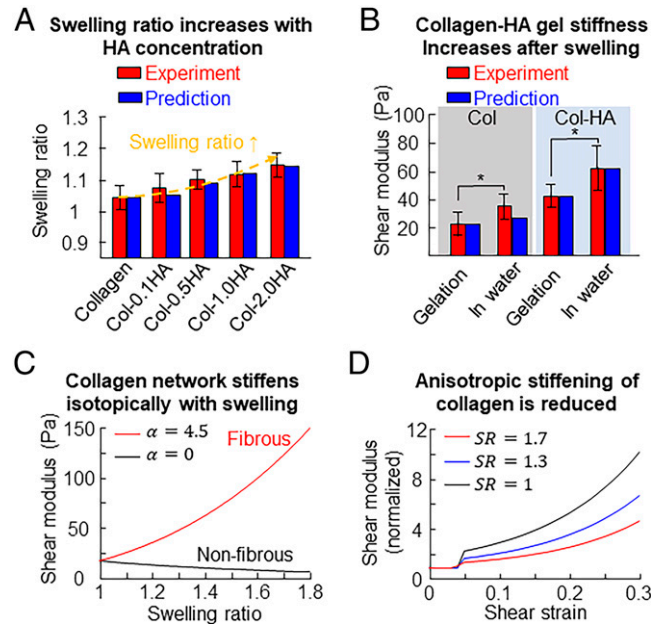


**Fig. 2.** Collagen (Col; 2.5 mg/mL) gels with varying amounts of HA (1.5 MDa, 0.1 to 2.0 mg/mL). (A) The change in gel volume following 24 h of submersion in pure water. An increase in HA concentration increases the swelling ratio, which is captured by the theoretical model. (B) The gel shear modulus (measured at 1% strain) before (after gelation) and after swelling (in deionized water); HA concentration 2.0 mg/mL. (C) The predicted change in the matrix shear modulus with swelling ratio. (D) The predicted change in the matrix shear modulus with shear strain, normalized to the instantaneous shear modulus.

by  $\Pi_{col}$  given in Eq. 17. While keeping the collagen concentration fixed at 2.5 mg/mL, we varied the amount of HA in the gel from 0.1 to 2.0 mg/mL. We found that the swelling ratio of collagen–HA gels increased from  $1.06 \pm 0.07$  to  $1.14 \pm 0.01$  as the concentration of HA increased. Using the free swelling ratio measured at different HA concentrations and the shear stiffness (*Collagen Network Stiffens Isotropically Due to Swelling Induced by GAGs*), we determined the model parameters  $\alpha$ ,  $\mu_{col}$ ,  $\kappa_{col}$ ,  $\mu_{GAG}$ ,  $\kappa_{GAG}$  as described in *SI Appendix, section 4*. The dependence of the swelling ratio on the HA concentration also agreed well with studies on tumor swelling, which have shown that tumors were no longer swollen after degradation of GAGs (13). We note that we mixed collagen and HA (1.5 MDa) without cross-linking agents when preparing the gels. The collagen–HA cogels should only contain physical entanglements between collagen and HA without chemical cross-links. A fraction of HA diffused out of the collagen network during swelling (*SI Appendix, Fig. S4*). Still, the HA constrained in the collagen network caused the gels to swell. The swelling observed in our experiments thus suggests that the collagen network can physically restrain the movement of large HA molecules.

**Collagen Network Stiffens Isotropically Due to Swelling Induced by GAGs.** Next, we investigated how swelling can change the stiffness of the collagen–GAG network. Our discrete fiber simulations revealed that when GAGs attract water to expand the collagen network, 1) the overall spatial density of collagen decreases, and 2) the fibers strain-stiffen upon the stretching of the initially wavy structures (Fig. 1B). The former causes a decrease of the network stiffness, similar to the effect of the decreasing stiffness of entropy-dominated polymer networks such as polyacrylamide as they swell (25). This mechanism competes with stiffening from the straightening of individual

fibers, and the ECM can either stiffen or soften depending on which mechanism is dominant. Our continuum model captured these behaviors well: The elasticity of the GAGs (Eq. 10) and the unaligned fibers (Eq. 12) is described by the nonfibrous constitutive law (Neo-Hookean), and both soften upon volume expansion. On the other hand, the scaling factor  $s(J)$ , determined from discrete fiber simulations, captures the stiffening effect (Eq. 13). Our model predicted that if the impact of straightening of collagen fibers is small (i.e.,  $\alpha \approx 0$  in the model), then the stiffness of the network decreases upon swelling. On the other hand, when  $\alpha$  (Eq. 13) is large, the collagen–GAG network transitions from softening to stiffening behavior upon swelling (Fig. 2C).

To identify whether the collagen–GAG network stiffens in physiologically relevant scenarios, we measured the storage (shear) modulus of the collagen–HA gels (see *Materials and Methods* for details). We fixed the collagen concentration at 2.5 mg/mL and the HA concentration at 2 mg/mL and let the gels swell freely for 24 h at room temperature. Before swelling, the collagen–HA gel ( $40 \pm 10$  Pa) was clearly ( $P < 0.001$ ) stiffer than the pure-collagen gel ( $22 \pm 10$  Pa), indicating that HA was physically linked to the collagen network, contributing to the elasticity of the collagen–HA cogel. This result agrees with data from the literature (5), which shows that the addition of HA can enhance the elasticity of the network. After swelling, we found that the collagen–HA gels became significantly ( $P < 0.001$ ) stiffer with an approximately twofold increase in shear stiffness to  $62 \pm 18$  Pa (Fig. 2B). This development was because the initially relaxed fibers in the collagen network became straightened and stretched in the process of swelling (26). Note that this stiffening behavior of the semiflexible collagen network is not present in polymeric hydrogels (e.g., cross-linked HA), where stiffness is dominated by the entropy of the flexible polymeric chains. Swelling can decrease the density of entropic springs and thus lead to softening. To compare the behavior of collagen networks and polymeric hydrogels, we conducted a separate free swelling experiment with nonfibrous HA gels. Note that these HAs were thiol-modified to form cross-linked gels, different from the linear HA in the collagen–HA cogels. After gelation, the shear modulus was measured to be  $243 \pm 20$  Pa. The stiffness decreased to  $186 \pm 11$  Pa after swelling in phosphate-buffered saline (PBS) (swelling ratio 1.3) and further decreased to  $138 \pm 20$  Pa after swelling in pure water (swelling ratio 3.3) (*SI Appendix*, Fig. S3). The softening of polymeric gels (e.g., styrene butadiene rubber, polyacrylamide) upon swelling has also been reported in previous studies (25, 27). Therefore, in contrast to collagen gels, nonfibrous gels did not stiffen upon swelling, validating the predictions of our theoretical model when  $\alpha = 0$  (Fig. 2C).

We used the measurements of stiffness and the free swelling ratio to quantitatively calibrate and validate our model for the elastic response of collagen–HA networks. We used a grid search to sweep the space of 5 parameters  $\alpha$ ,  $\mu_{col}$ ,  $\kappa_{col}$ ,  $\mu_{GAG}$ ,  $\kappa_{GAG}$  and chose the set that best fit (with the lowest mean squared error) the free swelling ratio (Fig. 2A) and shear moduli before and after swelling (Fig. 2B). Other parameters were obtained from the literature (see *SI Appendix*, section 6 table of parameters). With the parameters given in *SI Appendix*, section 6, our model quantitatively captured 1) the increase in the swelling ratio with increasing GAG concentration, and 2) the increase in network stiffness upon swelling (Fig. 2A and B). The excellent agreement between our simulations and experiments shows that for modest levels of swelling ( $SR = 1 \sim 1.2$ ), the stiffening induced by straightening fibers outpaces the softening due to a decrease in density, leading to an increase in matrix stiffness.

### Anisotropic Strain-Stiffening of Collagen Networks Is Less Prominent after Swelling.

Next, we studied the strain-stiffening behavior of the network at different levels of swelling. Using the model parameters obtained from the free swelling experiments, we further simulated shear deformation on the network at 3 levels of swelling ( $SR = 1$ ,  $SR = 1.3$ ,  $SR = 1.7$ ). After normalizing the shear modulus of the network with respect to the instantaneous shear modulus at zero shear strain, we compared the change of the shear modulus as a function of the shear strain. We found that as the initial swelling increases, the increase of the shear modulus is less apparent (Fig. 2D). At 0.3 shear strain, the shear modulus increased by 10 times compared with the instantaneous shear modulus when  $SR = 1$ . This level of stiffening was approximately twice as much as the case for  $SR = 1.7$ , which indicates that the strain-stiffening of the network is less prominent when the network is swollen. This is because 1) the swelling increases the stiffness of the network isotropically by stretching the fibers, and 2) anisotropic stiffening of the network due to fiber alignment is less affected by the isotropic expansion of the network. With an increase in the isotropic stiffness, the network becomes less nonlinear and the anisotropic stiffening is less prominent. Note that the kink in the curves (Fig. 2D) is due to the increase of network shear stiffness as fibers start to align along the directions of tension. On the other hand, we have previously identified that the strain-stiffening of the network along the direction of tension is essential to the long-range force transmission (2). Therefore, we predict that the range of force transmission decreases with network swelling, which can be induced by GAGs. In the next section, we present the analysis of the range of force transmission as a function of GAG content in the collagen network.

### Range of Cell Force Transmission Decreases with GAG Content.

Having identified the role of GAGs on the mechanics of collagen cogels, we proceeded to study how GAGs can alter the transmission of the active forces generated by cells. We first considered a simple case in which a contractile cell was embedded in a matrix with homogeneous distribution of GAGs. We modeled the cell as an ellipsoid described by the equation  $(x/a)^2 + (y/a)^2 + (z/b)^2 \leq 1$ , where  $a$  and  $b$  denote the half-length of the cell's short and long axes (Figs. 3A and 4A). We defined the cell aspect ratio,  $AR = b/a$ , which increases as the cell becomes elongated. To model the impact of cell shape (at fixed volume) on force transmission, we set  $a^2b = R_0^3$ . Here  $R_0$  is the radius of the cell when it assumes a spherical shape. In our previous study (2), we determined that the isotropic mechanical behavior of the unaligned collagen fibers cannot explain long-range force transmission; forces were transmitted at distances greater than the size of the cells due to the alignment of fibers in response to cellular forces. In our simulation setup, we let the ECM first swell freely under physiological conditions with  $\bar{c}_{H^+}$ ,  $\bar{c}_+$ ,  $\bar{c}_-$  on the outer boundary at 0.0001 mmol/L (pH = 7), 150 mmol/L, and 150 mmol/L, respectively. We then imposed a prescribed displacement boundary condition at the cell–ECM interface to simulate the contraction of the cell. Specifically, the cell contractile strains along the  $x$ ,  $y$ , and  $z$  directions ( $\epsilon_x$ ,  $\epsilon_y$ , and  $\epsilon_z$ , respectively) were set to be  $a^2(1 - \epsilon_x)(1 - \epsilon_y)b(1 - \epsilon_z) = R_0^3(1 - \epsilon_0)^3$ , so that the cell volume after contraction was the same for all shapes. Here  $\epsilon_0$  is a constant and  $\epsilon_x = \epsilon_y = \epsilon_z = \epsilon_0$  when the cell is spherical ( $AR = 1$ ). As shown by previous studies (3), the contraction of the cells becomes larger along their long axis as they become elongated, and therefore we assumed  $\epsilon_z/\epsilon_x = \epsilon_z/\epsilon_y = AR$ , so that the contractile strain was larger along the long axis for

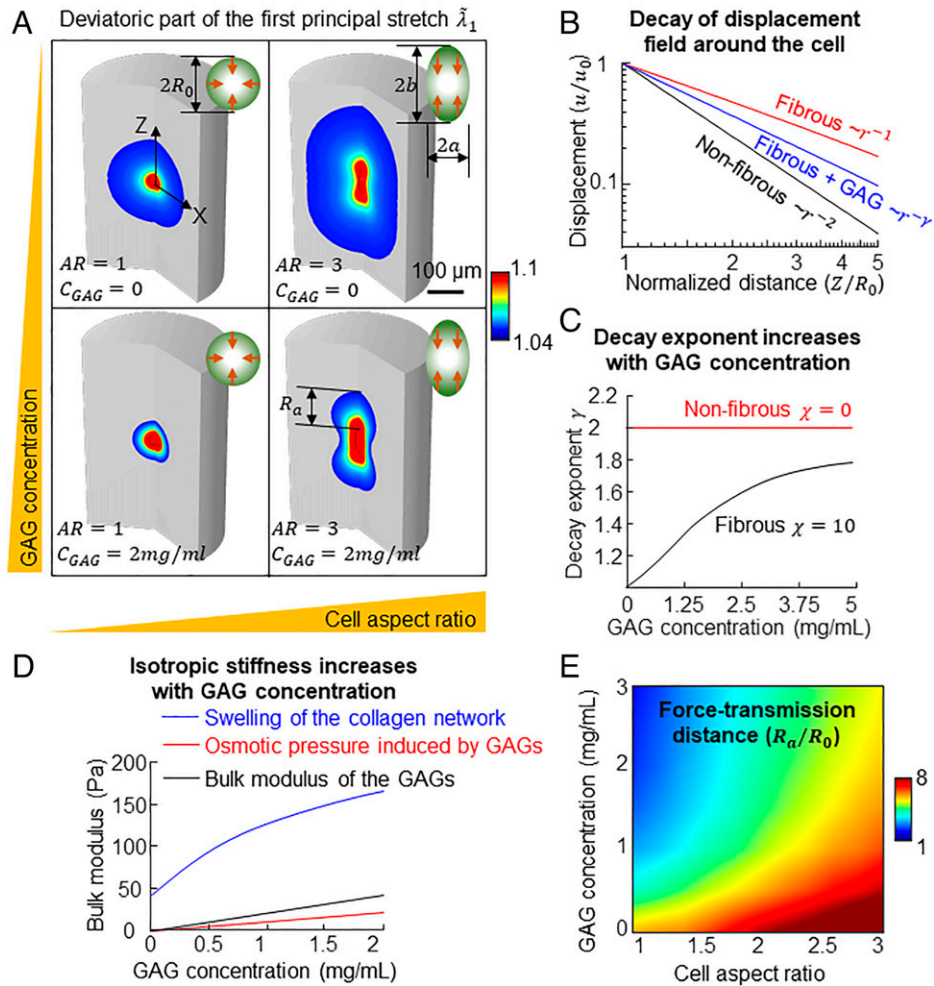


**Fig. 3.** (A) Influence of cell shape and GAG concentration on the distance ( $R_a$ ) over which the cell-induced contractile force is transmitted measured by the extent of the regions where fibers are aligned in matrices. We define aligned regions as part of the matrix with the deviatoric part of the first principal stretch larger than the critical value  $\bar{\lambda}_1 > \lambda_c$ . (Scale bar: 100  $\mu\text{m}$ .) (B) The decay of matrix displacement as a function of the distance from the cell. (C) Dependence of the decay exponent on GAG concentration. (D) Contribution to isotropic stiffness of the collagen–GAG cogels from 1) swelling of the collagen network, and 2) the bulk modulus of the GAGs and the osmotic pressure induced by the GAGs. (E) Heat map of the range of force transmission,  $R_a$ , as a function of cell shape and GAG concentration.

elongated cells. The outer boundary of the ECM was prescribed such that no displacement was allowed in directions perpendicular to the boundary. We ensured that the overall size of the simulation box was sufficiently large to eliminate boundary effects (matrix boundary to cell distance  $\gg 40R_0$ ). We repeated the simulations for various concentrations of GAGs and studied the range of force transmission.

With numerical simulations, we found that for a given level of cell contraction, there was a significantly decreased level of strain in the vicinity of the cell when GAGs were present (Fig. 3A) regardless of the cell shape. When the cell was spherical, the decay of the cell-induced displacement field  $u(r)$  was found to follow a power law  $u(r) \sim r^{-\gamma}$ , in which  $r$  denotes the distance to the center of the cell (2). In this case, we were able to derive an analytical expression for the decay exponent,

$$\gamma = \frac{1}{2} \left( 1 + \sqrt{\frac{9 + \xi}{1 + \xi}} \right), \quad [19]$$

where  $\xi = \frac{E_f}{\kappa + 4\mu/3}$  in which  $\kappa = s(J)\kappa_{col} + \frac{c_{GAG}}{c_{GAG}^{ref}}\kappa_{GAG} + d\Pi/dJ$  and  $\mu = s(J)\mu_{GAG} + \frac{c_{GAG}}{c_{GAG}^{ref}}\mu_{GAG}$  are the isotropic bulk and shear modulus of the GAG–collagen network that include

contributions from both the GAGs and unaligned collagen fibers. When there are no GAGs in the network,  $\xi = \frac{E_f}{\kappa_{col} + 4\mu_{col}/3}$ , where  $E_f$  (characterizing the anisotropic stiffening of the network) is much larger than the isotropic stiffness  $\kappa_{col}$  and  $\mu_{col}$ . In this case,  $\xi$  approaches infinity and the exponent  $\gamma$  approaches 1, indicating a slow decay of displacement. On the other hand,  $\gamma = 2$  when the network is not fibrous and thus does not strain-stiffen in an anisotropic manner ( $E_f = 0$ ,  $\xi = 0$ ). When GAGs are present in the network, the isotropic stiffness  $\kappa$  and  $\mu$  increase because GAGs directly contribute to the isotropic stiffness (captured by  $\kappa_{GAG}$  and  $\mu_{GAG}$ ) and induce swelling that stretches and stiffens the collagen network (captured by the scaling factor ( $s(J)$ )). In addition, compressing (stretching) the network leads to a higher (lower) concentration of fixed charges and thus a difference in osmotic pressure captured by  $d\Pi/dJ$ , which contributes to the bulk stiffness of the network (28). The contributions of these three mechanisms to the isotropic stiffness as a function of the GAG concentration is shown in Fig. 3D. We found that the contribution from the stiffening of the collagen network due to the swelling induced by GAGs was significantly larger than the other two mechanisms. With higher isotropic stiffness  $\kappa$  and  $\mu$  in the presence of GAGs, the decay exponent  $\gamma$  fell between

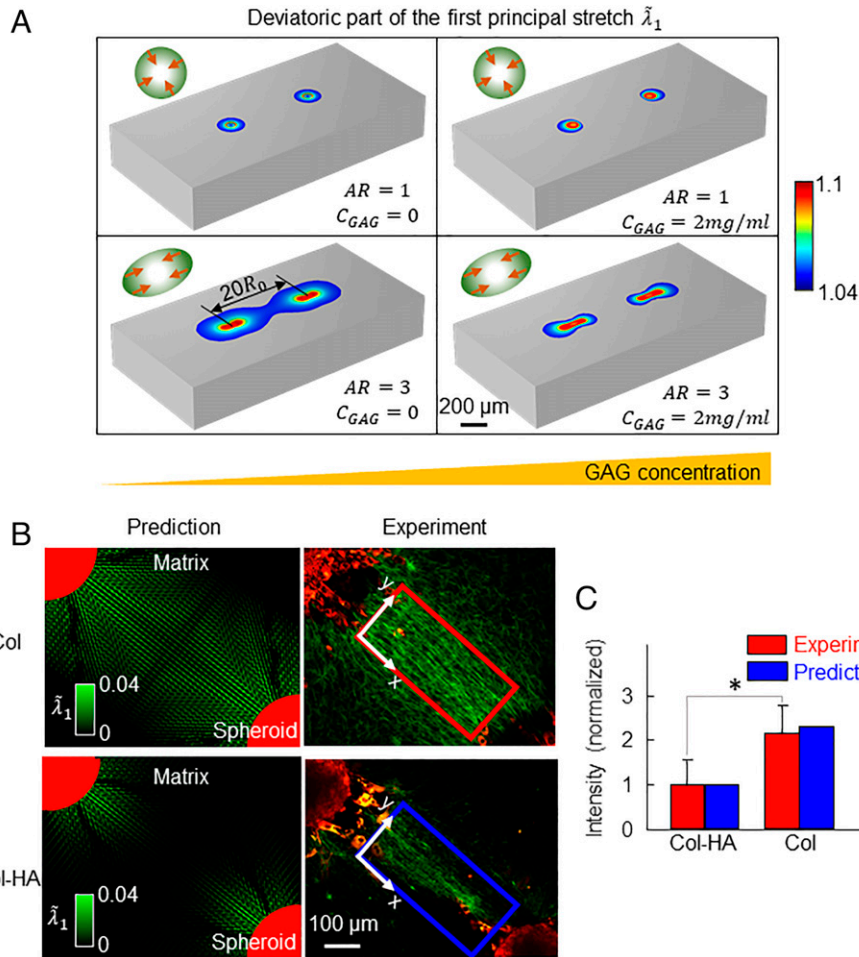


**Fig. 4.** (A) Theoretical prediction of fiber alignment between two cells in collagen–GAG cogels with increasing GAG concentration. (Scale bar: 200 μm.) (B) Theoretical prediction and experimental measurement of intensity of aligned collagen (Col) fibers between cell spheroids. (Scale bar: 100 μm.) (C) The average intensity of fiber alignment in the box specified in (B), as measured by ImageJ;  $n$  17 for collagen gels and  $n$  9 for collagen–HA gels, \* $P$  0.001. The theoretical prediction is derived from the average  $\tilde{\lambda}_1$ . The concentrations of collagen and HA were 2.5 mg/mL and 2 mg/mL, respectively.

1 and 2, with an increase in the value of the decay exponent with the concentration of GAGs as shown in Fig. 3C.

Since the cell-induced displacement decays faster when GAGs are present in the network, we also predicted a decrease in the range of force transmission. Through our numerical simulations, we found that the furthest distance that the cell-induced force could reach ( $R_a$ , defined by  $\tilde{\lambda}_1 = \lambda_c$ ) decreased with increasing GAG content in the network (Fig. 3A). To quantitatively investigate  $R_a$ , we conducted an analytical analysis (SI Appendix, section 2) and found that for a spherical cell,  $R_a$  could be calculated by

$$R_a = \sqrt[r+1]{-\frac{\gamma u_0 R_0^\gamma}{\lambda_c - 1}}. \quad [20]$$

Here,  $R_0$  denotes the radius of the cell, and  $u_0 = \varepsilon_0 R_0$  denotes the radial displacement at the cell–matrix interface. From this equation, it is apparent that the range of cell force transmission increases when the cell is more contractile (which can exert a higher displacement  $u_0$ ). For the same level of contraction  $u_0$ ,  $R_a$  decreases with the decay exponent  $\gamma$  (shown in SI Appendix, section 2). Therefore, we predict that the range of force transmission decreases with the concentration of GAGs as shown in Fig. 3A. Overall, high GAG concentration increases the isotropic stiffness of the collagen network and makes the anisotropic strain-stiffening less prominent. The network behavior approaches that

of a nonfibrous material (such as a linear elastic or Neo-Hookean material), in which the cellular force decays rapidly.

We then examined how the range of force transmission depends on GAGs when cells are elongated. Due to the anisotropy of the cell geometry and contractility (2), the contraction of an elongated cell caused a gourd-shaped region of fiber alignment (Fig. 3A). The elongated cell with an aspect ratio of 3 can transmit force more than 3 times farther than a round cell in a collagen matrix (Fig. 3A). Similar to the case of a round cell, when we increased the GAG concentration from 0 to 2 mg/mL, we found a significantly reduced range of force transmission. In Fig. 3E, we show the range of force transmission as a function of both GAG concentration and cell aspect ratio. For all the cell shapes that we investigated, GAGs reduced the range of cellular force transmission. A more comprehensive parametric study on the relation between the range of force transmission and other parameters ( $\chi$ ,  $\lambda_c$ , and  $u_0$ ) is included in SI Appendix, section 2. We found that the range of force transmission increased when 1) the collagen network strain-stiffened more, 2) the collagen network had a lower critical strain for alignment, and 3) the cell exerted larger levels of contractile forces (SI Appendix, Fig. S1).

**GAGs Suppress Long-Range Cell–Cell Communication.** Interactions between cells are involved in many biological processes (e.g., cancer cell invasion, wound healing, and fibrosis) and

play a significant role in the organization of tissues. Since the range of force transmission decreases in the collagen network with GAGs (as presented above), it is reasonable to expect that cell–cell interactions will also be impacted. To verify this hypothesis, we explicitly modeled the interaction between two contracting cells seeded on collagen substrates with varying amounts of GAGs. As in the case of single cells, where the deformation fields spread further from the cells when they were elongated, elongated cells interacted more significantly compared to spherical cells (Fig. 4). In the matrix without GAGs, we observed a significant overlap of regions of alignment between the two cells at a distance of 20 times  $R_0$  (Fig. 4A). The aligned regions were stiffened anisotropically along the line connecting the two cells, allowing efficient transmission of forces between the cells. However, with the addition of GAGs to the matrix, the regions of alignment no longer overlapped, indicating that the contraction of one cell cannot be felt by the other cell (Fig. 4A). Using these simulations, we confirmed that the cell–cell interaction distance was twice the size of the cell force transmission range, indicating that increasing GAG content can decrease long-range cell–cell communication.

To validate the prediction on the range of cellular force transmission, we measured the intensity of the aligned collagen fibers between two fibroblast spheroids. Since the cell aggregates remained roughly spherical (Fig. 4B) during the experiment, our model that considered two single spherical cells can be used here by treating each spheroid as a large single source of contractile force, which can be analyzed using the numerical and analytical methods shown in the model development section (*A Chemo-Mechanical Model of Cellular Force Transmission in Collagen Networks with Interpenetrating GAGs*) and *SI Appendix, section 2*. Fibroblast spheroids were seeded 600  $\mu\text{m}$  apart atop collagen type I gels (2.5 mg/mL) or collagen–HA cogels (2.5 mg/mL collagen and 2.0 mg/mL HA). The gels were formed on coverslips and exposed to the culture medium, after which fibroblasts began pulling the matrix following the formation of adhesions. Within a few hours, the contraction led to large-scale increases in the intensity of fiber alignment in the region connecting the two spheroids (Fig. 4B). We used second-harmonic generation (SHG) microscopy to visualize and image the intensity of the visibly aligned collagen fibers. Note that there are generally 2 approaches to experimentally estimating the relative orientation of collagen fibers using SHG imaging. The first, and much more common method, is through image (post) processing, where for sufficiently fibrous SHG images, common algorithms can be used to estimate fiber orientation (29–31). The second is through polarization-resolved measurements and appropriate system modeling (biological system plus focal volume [32, 33]). The latter approach is virtually impossible for commercial multiphoton microscopes as the optical train is inaccessible to end users, and care must be taken to factor in polarization-scattering effects when using high-numerical-aperture objectives (34–36). As a result, the image processing approach is the technique we employed, which is widely accepted to provide reasonable estimates of fiber orientation. We extracted the average SHG intensity along the  $y$ -direction and plotted it along the  $x$ -direction (Fig. 4B and C). We found that the increased intensity of aligned collagen was much less prominent between cells cultured on the collagen–HA gel, despite the fact that fibroblasts should be more contractile on the stiffer collagen–HA substrates (37). In contrast, without the cells, the collagen and collagen–HA gels showed comparable SHG intensity (*SI Appendix, Fig. S8*). This result suggests that GAGs decrease long-range force transmission in the matrix

and agrees very well with the intensity of aligned collagen fibers predicted by our model. We adopted the parameters determined from free swelling and rheology experiments (parameter values are listed in *SI Appendix, section 4*) and simulated the contraction of fibroblasts with 10% contractile strain. We visualized the deviatoric part of the first principal strain ( $\tilde{\lambda}_1$ ), whose magnitude indicates the density of aligned collagen, as shown in Fig. 4B. We found a quantitative agreement between the SHG intensity and the magnitude of the principal strain for both collagen and collagen–HA matrices (Fig. 4C). In Fig. 4C, we normalized the SHG intensity and  $\tilde{\lambda}_1$  by the values for the gels with collagen alone. The magnitude of the normalized value for the case of collagen gels reflects the fold-change of the intensity of aligned collagen in the highlighted box (Fig. 4B) compared with the case of collagen–HA gels.

We further experimented using a 3-dimensional configuration, where we seeded fibroblast spheroids within collagen (1.5 mg/mL) and collagen–HA (1.5 mg/mL and 1.0 mg/mL) cogels. For this case, we also found that the range of intensity of collagen fiber alignment significantly decreased in the presence of HA, consistent with our model prediction (*SI Appendix, Fig. S7*). The excellent quantitative agreement between model predictions and experiments confirms that the presence of GAGs indeed significantly modulates the range of force transmission in collagen matrices.

## Discussion

In this study, we developed and validated a theoretical model describing the mechanical behavior of collagen networks with interpenetrating GAGs. By combining predictions and experiments, we showed that GAGs can attract water into the ECM, stretching the collagen fibers and leading to an increase of network isotropic stiffness, and that the ECM becomes more resistant to volumetric changes. Collagen fibers stretched under swelling can better resist buckling and were less likely to align along the direction where the stresses were tensile (Fig. 5). For the same level of shear load, the anisotropy of the fiber orientation decreased with the swelling ratio. By preventing the reorientation of collagen fibers that is essential to long-range force transmission, GAGs decreased long-range force transmission. Note that the increasing bending stiffness of collagen fibers was previously shown to also hamper the range for force transmission by preventing buckling. However, the effect of collagen network swelling showed a distinct scaling relation between network stiffness and strain. We show in *SI Appendix, section 5* that the network stiffening by increasing fiber bending stiffness was significantly smaller than what was caused by fiber stretching; the impact of a modest 10% volumetric swelling strain was on par with an increasing bending modulus by a large factor of 100. In agreement with our model predictions, we found significant decreases in the intensity of aligned collagen between cell spheroids in collagen–HA cogels compared with collagen gels. We further showed that the local accumulation of GAGs can create barriers to cellular force transmission (*SI Appendix, Fig. S2*). This finding is physiologically relevant because the distribution of GAGs can be highly inhomogeneous in vivo. For example, in breast tumors, high concentrations of GAGs are only observed at the leading edge of the tumor (7), and the localization of GAGs has been linked to the severity of cancer.

While we experimentally validated our model using HA as the model GAG, the ECM in vivo also contains other types of GAGs such as chondroitin sulfate and heparan sulfate. Often, GAGs attach to core proteins to form proteoglycans, such as

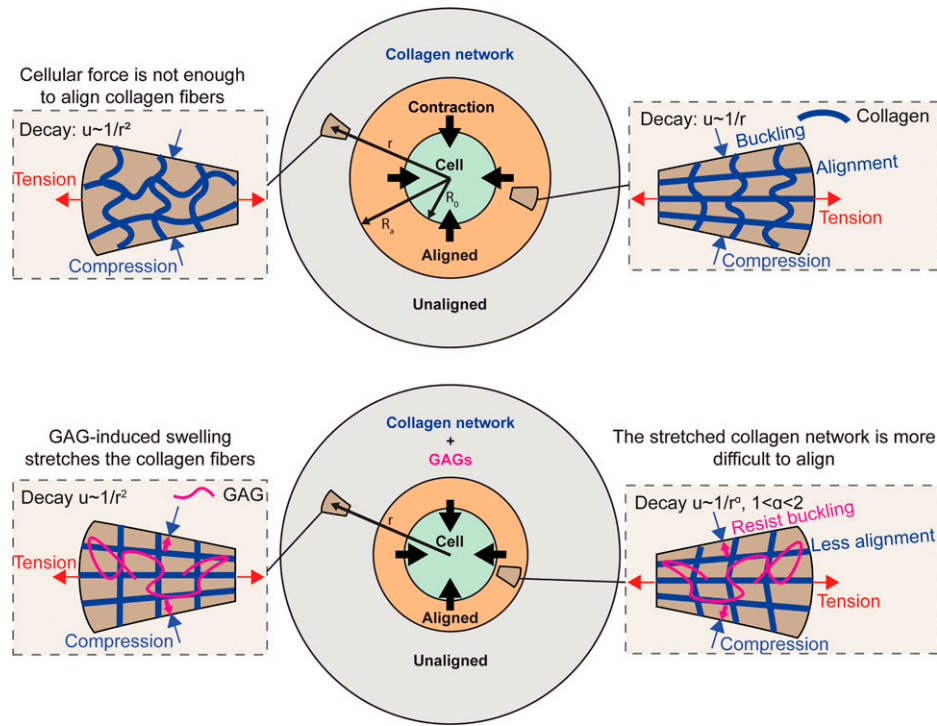


**Fig. 5.** Schematic showing the role of GAGs in cellular force transmission. In the matrix without GAGs (*Top*), contraction of the cell aligns the fibers in the radial direction. Here  $u$  denotes the radial displacement and  $r$  denotes the distance from the cell. In the presence of GAGs, collagen networks are better able to resist compression and buckling in the transverse direction. This mechanism reduces collagen fiber alignment in the radial direction and reduces the efficiency of force transmission.

the highly GAG-modified bottle-brush aggrecan, which is further bound to HA chains to form a larger proteoglycan complex (38). Like HA, these GAGs contain acidic groups (e.g., carboxyl, sulfate) that can dissociate into fixed negative charges and induce swelling with the same mechanism (10). Therefore, the theoretical predictions in this study can be applied to other GAGs that can attract water and swell the matrix. However, in native ECM, the content of free GAGs and PG (proteoglycan)-bound GAGs is still unclear. As different PGs appear to interact differently with collagen (39), PG-bound GAGs (fixed-charge residues) may have complicated effects on the mechanical communication between cells. Thus, there is a particular need to investigate and compare the regulation of free versus PG-bound GAGs on the fibrous network as one future direction for modeling force transmission in native ECM.

Our results have implications for cellular mechano-transduction in biological systems where GAGs are involved. For example, cancer-associated fibroblasts (CAFs) behave very differently than their normal counterparts in ways that allow them to thrive and contribute to the development of the tumor microenvironment (10). One of the important distinctions between the two kinds of fibroblasts is that CAFs have a significantly increased ability to synthesize HA (40). GAGs are also abundant in connective tissues such as cartilage and tendon. These tissues undergo constant mechanical loading, and GAGs are critical to maintain the hydration necessary for them to function normally. Damaged cartilage usually shows decreased GAG content. Our model provides a foundation for the analysis of cell mechano-sensing in these scenarios and can potentially help develop treatments for disease conditions related to changes in GAG content (41).

In this study, our focus has been on the impact of GAGs on cellular force transmission. However, GAGs also play a role in mechano-sensing by attaching to cell membrane receptors such

as the HA receptors CD44 and RHAMM (*SI Appendix, Fig. S2A*). GAGs are a major component of the pericellular matrix (PCM), also known as the glycocalyx (9), which can extend as much as 20  $\mu\text{m}$  from the cell surface. An osmotic pressure gradient has been experimentally observed (42) in the PCM as the density of GAG chains increases approaching the cell surface, and this gradient may be relevant in cell mechano-sensing. For example, several studies have shown that HA in the PCM can have both adhesive (43, 44) and antiadhesive (45–47) roles. Surface HA is also involved in transducing shear stress to endothelial cells (48). HA up-regulates the contractility of periodontal ligament cells via its interaction with CD44 (49). We hope to further investigate these roles of GAGs in forthcoming work.

## Materials and Methods

**Gel Preparation and Free Swelling Experiments.** Collagen-HA gels were prepared by mixing rat tail collagen I (Corning) to a final concentration of 2.5 mg/mL with a varying amount of HA (collagen-to-HA weight ratio: 2.5:0.1, 2.5:0.5, 2.5:1, and 2.5:2; 1.5 MDa sodium hyaluronate from Lifecore Biomedical). The gel solutions were incubated at 37 °C overnight and were then submerged in deionized water at room temperature, subject to no force. After 24 h, we wiped excessive water from the gel surface and measured the weight. The swelling ratio (SR) was then calculated by

$$SR = 1 + \frac{(m_{\text{swollen}} - m_{\text{initial}}) / \rho_{\text{water}}}{m_{\text{initial}} / \rho_{\text{gel}}}, \quad [21]$$

where  $m_{\text{initial}}$  and  $m_{\text{swollen}}$  denote the weight of the gel before and after swelling, respectively.  $\rho_{\text{water}}$  and  $\rho_{\text{gel}}$  denote the density of water and gel prior to swelling, respectively. As the mass concentrations of collagen and hyaluronan are less than 1%, we assumed that  $\rho_{\text{gel}} \approx \rho_{\text{water}}$ . Note that the HA used here was not cross-linked and only was physically restrained in the collagen network. After 24 h, almost 50% of the hyaluronan had diffused out of the gel (*SI Appendix, Fig. S5*). However, the HA that remained in the collagen gel network still induced swelling compared to the pure collagen (Fig. 2A). Cross-linked HA hydrogel was made by mixing Glycosil (thiol-modified HA from Advanced BioMatrix) with

Extralink (thiol-reactive crosslinker, polyethylene glycol diacrylate) at a volume ratio of 4:1 and was formed on a 20 mm coverslip. The swelling experiments were carried out as described above.

**Shear Rheology Experiments.** For the rheometry of collagen, collagen-HA, and cross-linked HA gels, the gel solutions were prepared as previously described for the free swelling experiments. Unswollen gels were measured after gelation and swollen gels were measured after swelling in deionized water for 24 h. A shear rheometer (Kinexus) with rSpace software was used to characterize shear modulus. A 20 mm plate was used, and both storage and loss ( $G'$  and  $G''$ ) were measured by applying an oscillatory shear strain of 2% at a frequency of 10 rad/s (1.592 Hz).

**Fibroblast Spheroid Experiment.** Collagen and collagen-HA gels were prepared as described for the free swelling experiments using microwell plates with glass-bottomed cutouts. Plates were sealed with parafilm and kept in an incubator overnight at 37 °C. Fibroblast spheroids were formed by the hanging droplet method. Briefly, passaged rat portal fibroblasts (50) were trypsinized and suspended in culture media at 200,000 cells/mL. Next, 20  $\mu$ L droplets of suspension cell solution was placed on the underside of a dish lid. To avoid drying, 10 mL media was added to the dish. After inversion of the lid, the cell droplets were cultured for 3 d. For seeding, spheroids were captured and carefully placed on the gel in pairs  $\sim$ 600  $\mu$ m apart. The gel was incubated for 4 h, allowing the spheroids to attach, and then 2 mL media was added. After culturing for another 20 h, gels were rinsed with PBS and fixed with 10% formalin for 10 min. All the samples were sealed with parafilm and kept in PBS at 4 °C. SHG imaging was used to visualize collagen fibers (39). ImageJ was used to determine the intensity of the aligned collagen in the defined regions either between spheroids or at distant sites.

**Statistical Analysis.** The significance of changes in shear moduli and swelling ratio were tested using a 1-way ANOVA; SHG intensities were compared using the Student's  $t$  test (unpaired). The  $P$  value was chosen to be 0.001.

**Discrete 3-Dimensional Fiber Network Model.** We generated 3-dimensional fiber networks by placing fibers over the edges of a 3-dimensional Voronoi tessellation. The Voronoi diagrams were generated by random seed points using MATLAB (MathWorks, Natick, MA). The individual fibers were modeled as Timoshenko beams (51), flexible in bending, stretching, twisting, and shear modes

of deformation. Fiber waviness was introduced by shaping each fiber into a half-sine wave. The amplitude of the sine waves equaled half of the fiber end-to-end length. The fibers had circular cross-sections of diameter 150 nm and elastic moduli of 6.5 MPa. Implicit finite element calculations were performed using the Abaqus software package (Simulia). The shear tests were performed by the horizontal displacement of the top surface, in the  $x$  direction, while the bottom was held fixed. The shear tests of the expanded networks were performed in 2 steps. In the first step, the volumetric expansion of the networks was modeled by the stretching of the networks equally in 3 directions by enforcing displacements at the boundaries. The reaction forces at the boundary nodes over all surfaces except the top and bottom surfaces were recorded at the expanded state using the Abaqus scripting interface in Python. In the second step, displacement boundary conditions were applied to the nodes on the top and bottom surfaces, while the recorded reaction forces due to volumetric expansion were applied to the nodes on all surfaces except for the top and bottom surfaces. Fiber reorientation was characterized by the measurement of the distribution of the orientation of fibers stretched by more than 1%. The orientation of individual fibers was evaluated by the projection of the fiber's end-to-end vector onto the front surface of the network and the calculation of the orientation of the projected vector with respect to the  $x$ -direction.

**Data Availability.** All study data are included in the article and/or *SI Appendix*.

**ACKNOWLEDGMENTS.** This work was supported by National Cancer Institute awards R01CA232256 (V.B.S.) and U54CA261694 (V.B.S.), National Institute of Biomedical Imaging and Bioengineering awards R01EB017753 (V.B.S., R.G.W., P.A.J.) and R01EB030876 (V.B.S.), NSF Center for Engineering Mechanobiology grant CMMI-154857 (R.G.W., P.A.J., V.B.S.), and NSF grants MRSEC/DMR-1720530 (R.G.W., P.A.J., V.B.S.) and DMS-1953572 (V.B.S.).

Author affiliations: <sup>a</sup>Center for Engineering MechanoBiology, University of Pennsylvania, Philadelphia, PA 19104; <sup>b</sup>Department of Materials Science and Engineering, University of Pennsylvania, Philadelphia, PA 19104; <sup>c</sup>Department of Bioengineering, University of Pennsylvania, Philadelphia, PA 19104; <sup>d</sup>Department of Biomedical Engineering, Yale University, New Haven, CT 06520; <sup>e</sup>School of Engineering, Brown University, Providence, RI 02912; <sup>f</sup>Department of Physiology, University of Pennsylvania, Philadelphia, PA 19104; and <sup>g</sup>Department of Medicine, University of Pennsylvania, Philadelphia, PA 19104

1. C. Frantz, K. M. Stewart, V. M. Weaver, The extracellular matrix at a glance. *J. Cell Sci.* **123**, 4195–4200 (2010).
2. H. Wang, A. S. Abhilash, C. S. Chen, R. G. Wells, V. B. Shenoy, Long-range force transmission in fibrous matrices enabled by tension-driven alignment of fibers. *Biophys. J.* **107**, 2592–2603 (2014).
3. H. Ahmadzadeh *et al.*, Modeling the two-way feedback between contractility and matrix realignment reveals a nonlinear mode of cancer cell invasion. *Proc. Natl. Acad. Sci. U.S.A.* **114**, E1617–E1626 (2017).
4. S.-L. Xue, S.-Z. Lin, B. Li, X.-Q. Feng, A nonlinear poroelastic theory of solid tumors with glycosaminoglycan swelling. *J. Theor. Biol.* **433**, 49–56 (2017).
5. V. K. Lai *et al.*, Swelling of collagen-hyaluronic acid co-gels: An in vitro residual stress model. *Ann. Biomed. Eng.* **44**, 2984–2993 (2016).
6. M. K. Cowman, H.-G. Lee, K. L. Schwertfeger, J. B. McCarthy, E. A. Turley, The content and size of hyaluronan in biological fluids and tissues. *Front. Immunol.* **6**, 261 (2015).
7. P. Auvinen *et al.*, Hyaluronan in peritumoral stroma and malignant cells associates with breast cancer spreading and predicts survival. *Am. J. Pathol.* **156**, 529–536 (2000).
8. N. Bouhrira, P. A. Galie, P. A. Janmey, Hyaluronan disrupts cardiomyocyte organization within 3D fibrin-based hydrogels. *Biophys. J.* **116**, 1340–1347 (2019).
9. J. Chin-Hun Kuo, J. G. Gandhi, R. N. Zia, M. J. Paszek, Physical biology of the cancer cell glycocalyx. *Nat. Phys.* **14**, 658–669 (2018).
10. W. M. Lai, J. S. Hou, V. C. Mow, A triphasic theory for the swelling and deformation behaviors of articular cartilage. *J. Biomech. Eng.* **113**, 245–258 (1991).
11. H. Li, S. R. Sun, J. Q. Yap, J. H. Chen, Q. Qian, 0.9% saline is neither normal nor physiological. *J. Zhejiang Univ. Sci. B* **17**, 181–187 (2016).
12. A. Philipse, A. Vrij, The Donnan equilibrium: I. On the thermodynamic foundation of the Donnan equation of state. *J. Phys. Condens. Matter* **23**, 194106 (2011).
13. C. Voutouri, C. Polydorou, P. Papageorgis, V. Gkretsi, T. Stylianopoulos, Hyaluronan-derived swelling of solid tumors, the contribution of collagen and cancer cells, and implications for cancer therapy. *Neoplasia* **18**, 732–741 (2016).
14. R. Marcombe *et al.*, A theory of constrained swelling of a pH-sensitive hydrogel. *Soft Matter* **6**, 784–793 (2010).
15. M. Raspanti *et al.*, Glycosaminoglycans show a specific periodic interaction with type I collagen fibrils. *J. Struct. Biol.* **164**, 134–139 (2008).
16. H. Munakata, K. Takagaki, M. Majima, M. Endo, Interaction between collagens and glycosaminoglycans investigated using a surface plasmon resonance biosensor. *Glycobiology* **9**, 1023–1027 (1999).
17. A. Varki *et al.*, *Proteoglycans and Glycosaminoglycans. Essentials of Glycobiology* (Cold Spring Harbor Laboratory Press, Cold Spring Harbor, NY, 1999).
18. F. Burla, J. Tauber, S. Dussi, J. van Der Gucht, G. H. Koenderink, Stress management in composite biopolymer networks. *Nat. Phys.* **15**, 549–553 (2019).
19. E. Ban *et al.*, Strong triaxial coupling and anomalous Poisson effect in collagen networks. *Proc. Natl. Acad. Sci. U.S.A.* **116**, 6790–6799 (2019).
20. E. Ban *et al.*, Mechanisms of plastic deformation in collagen networks induced by cellular forces. *Biophys. J.* **114**, 450–461 (2018).
21. N. R. Lang *et al.*, Estimating the 3D pore size distribution of biopolymer networks from directionally biased data. *Biophys. J.* **105**, 1967–1975 (2013).
22. A. J. Licup *et al.*, Stress controls the mechanics of collagen networks. *Proc. Natl. Acad. Sci. U.S.A.* **112**, 9573–9578 (2015).
23. S. Morozova, M. Muthukumar, Electrostatic effects in collagen fibril formation. *J. Chem. Phys.* **149**, 163333 (2018).
24. A. Mero, M. Campisi, Hyaluronic acid bioconjugates for the delivery of bioactive molecules. *Polymers (Basel)* **6**, 346–369 (2014).
25. Y. Hu, J.-O. You, D. T. Auguste, Z. Suo, J. J. Vlassak, Indentation: A simple, nondestructive method for characterizing the mechanical and transport properties of pH-sensitive hydrogels. *J. Mater. Res.* **27**, 152–160 (2012).
26. M. L. Oyen *et al.*, Uniaxial and biaxial mechanical behavior of human amnion. *J. Mater. Res.* **20**, 2902–2909 (2005).
27. Y. Lou, A. Robisson, S. Cai, Z. Suo, Swellable elastomers under constraint. *J. Appl. Phys.* **112**, 034906 (2012).
28. X. L. Lu, L. Q. Wan, X. E. Guo, V. C. Mow, A linearized formulation of triphasic mixture theory for articular cartilage, and its application to indentation analysis. *J. Biomech.* **43**, 673–679 (2010).
29. R. A. R. Rao, M. R. Mehta, K. C. Toussaint Jr., Fourier transform-second-harmonic generation imaging of biological tissues. *Opt. Express* **17**, 14534–14542 (2009).
30. W. Lee *et al.*, Quantitative classification of 3D collagen fiber organization from volumetric images. *IEEE Trans. Med. Imaging* **39**, 4425–4435 (2020).
31. A. C. Salazar Coariti *et al.*, Fluid mechanics approach to analyzing collagen fiber organization. *J. Biomed. Opt.* **27**, 016503 (2022).
32. P. Stoller, K. M. Reiser, P. M. Celliers, A. M. Rubenchik, Polarization-modulated second harmonic generation in collagen. *Biophys. J.* **82**, 3330–3342 (2002).
33. D. G. Winters, D. R. Smith, P. Schlup, R. A. Bartels, Measurement of orientation and susceptibility ratios using a polarization-resolved second-harmonic generation holographic microscope. *Biomed. Opt. Express* **3**, 2004–2011 (2012).

34. A. F. Abouraddy, K. C. Toussaint Jr., Three-dimensional polarization control in microscopy. *Phys. Rev. Lett.* **96**, 153901 (2006).
35. L. Novotny, M. R. Beversluis, K. S. Youngworth, T. G. Brown, Longitudinal field modes probed by single molecules. *Phys. Rev. Lett.* **86**, 5251–5254 (2001).
36. B. Richards, E. Wolf, Electromagnetic diffraction in optical systems, II. Structure of the image field in an aplanatic system. *Proc. R. Soc. Lond. A Math. Phys. Sci.* **253**, 358–379 (1959).
37. V. B. Shenoy, H. Wang, X. Wang, A chemo-mechanical free-energy-based approach to model durotaxis and extracellular stiffness-dependent contraction and polarization of cells. *Interface Focus* **6**, 20150067 (2016).
38. V. C. Mow, X. E. Guo, Mechano-electrochemical properties of articular cartilage: Their inhomogeneities and anisotropies. *Annu. Rev. Biomed. Eng.* **4**, 175–209 (2002).
39. D. Chen *et al.*, Distinct effects of different matrix proteoglycans on collagen fibrillogenesis and cell-mediated collagen reorganization. *Sci. Rep.* **10**, 19065 (2020).
40. K. L. Schwertfeger, M. K. Cowman, P. G. Telmer, E. A. Turley, J. B. McCarthy, Hyaluronan, inflammation, and breast cancer progression. *Front. Immunol.* **6**, 236 (2015).
41. B. R. Freedman *et al.*, Dynamic loading and tendon healing affect multiscale tendon properties and ECM stress transmission. *Sci. Rep.* **8**, 10854 (2018).
42. L. T. McLane *et al.*, Spatial organization and mechanical properties of the pericellular matrix on chondrocytes. *Biophys. J.* **104**, 986–996 (2013).
43. T. S. Wilkinson, S. L. Bressler, S. P. Evanko, K. R. Braun, T. N. Wight, Overexpression of hyaluronan synthases alters vascular smooth muscle cell phenotype and promotes monocyte adhesion. *J. Cell. Physiol.* **206**, 378–385 (2006).
44. W. Selbi *et al.*, Characterization of hyaluronan cable structure and function in renal proximal tubular epithelial cells. *Kidney Int.* **70**, 1287–1295 (2006).
45. B. J. Barnhart, S. H. Cox, P. M. Kraemer, Detachment variants of Chinese hamster cells. Hyaluronic acid as a modulator of cell detachment. *Exp. Cell Res.* **119**, 327–332 (1979).
46. G. Abatangelo, R. Cortivo, M. Martelli, P. Vecchia, Cell detachment mediated by hyaluronic acid. *Exp. Cell Res.* **137**, 73–78 (1982).
47. S. Koochekpour, G. J. Pilkington, A. Merzak, Hyaluronic acid/CD44H interaction induces cell detachment and stimulates migration and invasion of human glioma cells in vitro. *Int. J. Cancer* **63**, 450–454 (1995).
48. S. Mochizuki *et al.*, Role of hyaluronan glycosaminoglycans in shear-induced endothelium-derived nitric oxide release. *Am. J. Physiol. Heart Circ. Physiol.* **285**, H722–H726 (2003).
49. Z. Al-Rekabi *et al.*, Hyaluronan-CD44 interactions mediate contractility and migration in periodontal ligament cells. *Cell Adhes. Migr.* **13**, 138–150 (2019).
50. J. W. Wen, A. L. Olsen, M. Perepelyuk, R. G. Wells, Isolation of rat portal fibroblasts by in situ liver perfusion. *J. Vis. Exp.* **64**, e3669 (2012).
51. D. L. Logan, K. Chaudhry, *A First Course in the Finite Element Method* (Cengage Learning, Boston, MA, 2011).